TUNING ELLIPTICAL NIOBIUM CAVITIES BY PLASTIC DEFORMATIONS *

Valery Shemelin†, Joe Conway
Cornell Laboratory for Accelerator-based Sciences and Education (CLASSE), Ithaca, NY 14853

Abstract

The niobium superconducting accelerating cavities used in many contemporary accelerators require tuning to a working frequency after fabrication. This tuning is necessary because small variations between cells can substantially alter the field profile and decrease the accelerating rate. ANSYS simulations are done to understand changing of the initial shape due to plastic deformations at tuning. Simulations are presented for inner cells of a multicell cavity and for the end group including the end cell and the beam pipe. The tuning device has different contact areas on the cell surface where the force is applied, so stretching and squeezing the cavity cell are studied separately. The influence of the stiffening rings is also studied. The cavity tuned to the working frequency with the tuning device has a shape different from the designed shape. So, parameters of the higher order modes (HOMs) excited by the beam will also differ from the parameters calculated for the designed shape. Knowledge of these disturbed parameters is necessary for calculations of the beam breakup caused by HOMs.

INTRODUCTION

If the accelerating cavity has more than one cell, the cells need to be tuned relative to each other so that the accelerating field is the same in each cell [1]. Each cell is tuned by squeezing or stretching it in a special device. The place of the contact between this device and the cell is different for squeezing and stretching, so the deformations can occur in the different places along the cell. These tuning deformations are of necessity plastic, contrary to elastic deformations used for cavities in the cryomodule when a fine tuning is needed. Deformations discussed in [2] were calculated for the elastic case. A more general approach with the plastic deformations is needed.

A multicell cavity for high β values has different inner and end cells, Fig. 1. The inner cell is usualy symmetric relative to the left and right side, so each halfcell can be described by 7 parameters related to the inner surface that define the RF properties of the cell: equatorial radius R_{eq}, radius of aperture R_a, length L, half-axis of the equatorial and iris elliptic arcs: A, B, a, and b, respectively, Fig.2. There is a straight segment l between the arcs, the wall slope angle α is usually chosen $> 90^\circ$ for easier drainage of chemical liquids at the preparation of the surface.

* Supported by NSF award DMR-0807731
† vs65@cornell.edu

First of all, we will analyze deformations of the inner cell on the example of the Cornell ERL accelerating cavity with inner dimensions presented in Fig. 2. Wall thickness can be different in different points of a cell due to the procedure of stamping from a flat sheet niobium. For simplicity we will take a uniform thickness of 3 mm. Actual thickness varies from approximately 2.8, at the iris, to 3.2 mm, at the equator [3].

Then we will discuss the mechanical properties of the cavity with stiffening rings and of the end group that consists of the cell and a beam pipe.

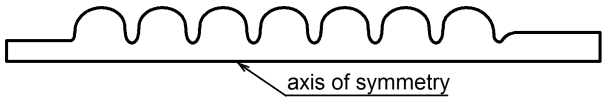

Figure 1: Multicell elliptic cavity.

The problem of HOMs parameters scatter due to the deviations of the shape from the design was discussed in [4]. Initially, random deviations of the elliptic half-axes were introduced, then tuning by changing the length of the cell was done. It was supposed that the half-axes and radii of the equator and aperture do not change in the process of this tuning.

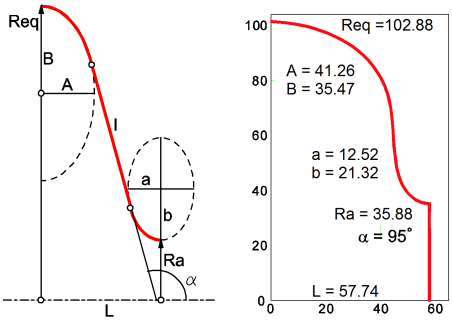

Figure 2: Parameters of the inner halfcell and dimensions of the inner halfcell of the Cornell ERL main linac. Dimensions, in mm, are given for the production drawings, before etching, at room temperature.

As can be found from the data published in [2], the fundamental frequency change in the case of elastic deformation is $df/dL = 5.9$ MHz/mm, whereas the above mentioned simplified model from [4] gives $df/dL = 3.9$ MHz/mm. This means that the parameters of HOMs will also change differently in the process of elastic tuning than in the simplified model. We can be sure that the plastic de-

formations will also be quite different from the elastic ones, moreover from the simplified model.

We will suggest, like in [2] and [4], that the deformed cavity is still the elliptic cavity, i.e. can be described by two elliptic arcs connected with a straight segment tangent to the arcs at the points of connection. However, we will evaluate the deviation from the elliptic model because for large deformations this model can become unsatisfactory.

The design of the tuning device for plastic deformations can have a decisive effect on the values of deformation. The plates which contact the cell walls are different for the cavities with and without stiffening rings.

Calculations were performed with the ANSYS structural mechanics software [5].

MECHANICAL PROPERTIES OF NIOBIUM

Summary of mechanical properties of niobium was compiled in [6]. The data presented here from various sources are sometimes contradicting and depend on many different conditions: RRR, heat treatment – temperature and duration of annealing, grain size, mechanical processing. The electron welded iris area can also have different mechanical properties compared to the rest part of the cavity cell. These details can be taken into account in future research. To the best of our knowledge this research is the first on simulating the process of tuning the acceleration cavity, so we will chose a definite set of properties to find the most general features of the cell behaviour in the process of plastic deformation.

For our simulations we used the model with the bilinear isotropic hardening and the following parameters of the material were taken: Yield Strength = $5 \cdot 10^7$ Pa, Tangent Modulus = $2 \cdot 10^9$ Pa, Young Modulus = $5 \cdot 10^{10}$ Pa, Fig. 3.

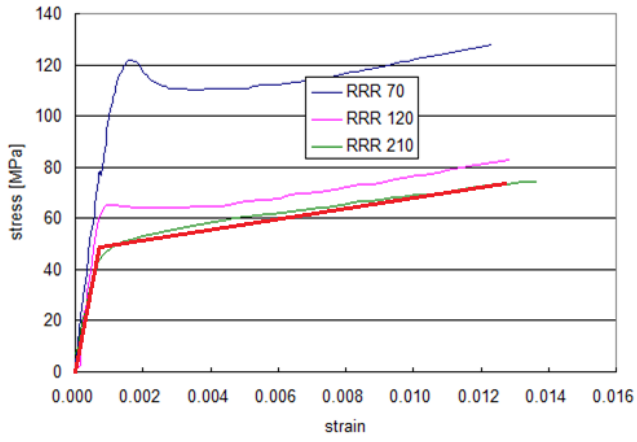

Figure 3: Reactor grade niobium with RRR = 70; 1200 C 6 hour with RRR = 120; 1250 C 6 hour with RRR = 210; crystal grain size unknown [6]. The bold red line is the approximation for our simulations.

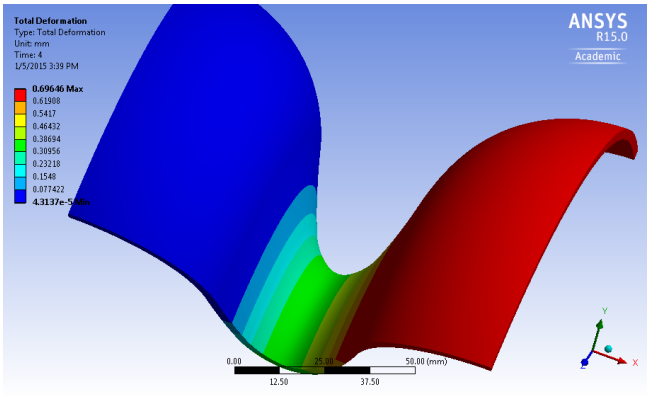

Figure 4: Deformation of the dumbbell stretched by a force of 7 kN.

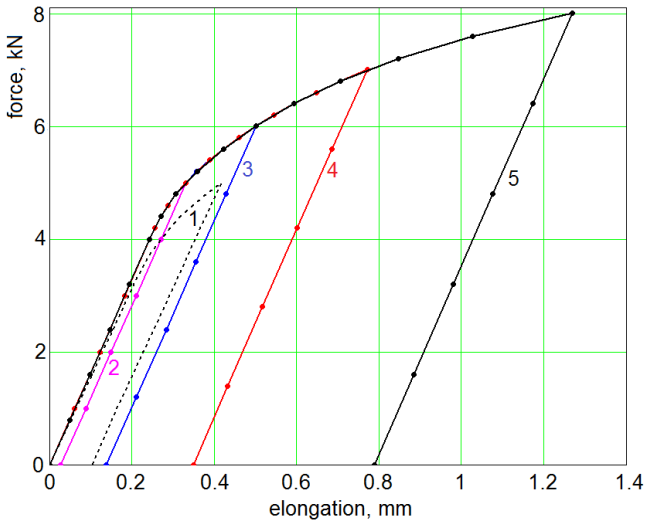

Figure 5: Elasto-plastic behavior of the halfcell with a free end at the iris (1) and as part of a dumbbell for maximal stretching force from 5 to 8 kN (2 – 5).

STRETCHING AN INNER CELL WITHOUT STIFFENING RINGS

For the simplest case of stretching a cell without stiffening rings we have to take a dumbbell – two halfcells having a common iris. The model used for calculations is shown in Fig. 4. Because of axial symmetry one quarter only of the whole dumbbell was considered in most cases. The dumbbell is fixed at the plane passing through its equator on the left side but can move in the radial direction. The force is applied uniformly and parallel to the axis of rotation to the cross-section passing through the right equatorial plane. If the model consists of a halfcell only (left half of the model in Fig. 4) and the force is applied to the iris cross-section, the iris has no constrains in the radial direction, and the iris part of the halfcell starts to bend out of the axis of rotation leading to results very different from the results with a dumbbell model.

In Fig. 5, the values of the halfcell elongation are shown

for different maximal forces applied to the halfcell or to the dumbbell. Deformations of different parts of the dumbbell are shown in Fig. 4, and the residual stresses are presented in Fig. 6.

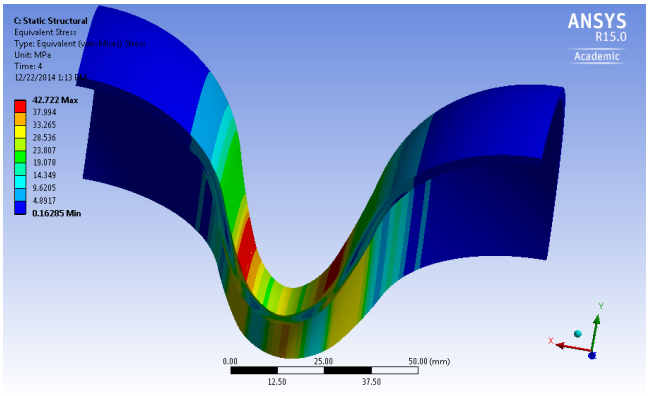

Figure 6: Residual stress of the dumbbell stretched by a force of 7 kN.

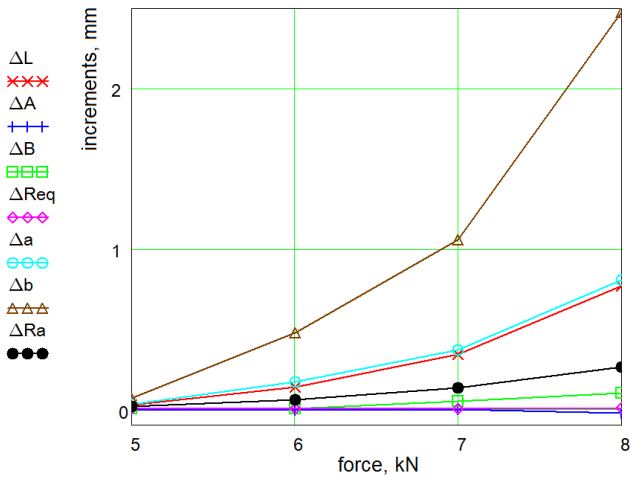

Figure 7: Residual deformation of the unstiffened halfcell vs applied stretching force.

One can see that the deformation occurs mainly in the iris region, the equatorial region is practically not deformed and has no residual stress. This is also seen in Fig. 7 where the increments of the geometric parameters of the halfcells are presented after application of different maximal forces. These dependences on force are very strong starting from some point, but if we plot these increments for different increments of the halfcell length ΔL, we can see that they are practically linear, Fig. 8. On the same Fig. 8 the values of the rms deviation σ from the elliptic shape are presented. One can see that σ is more than 3 orders of magnitude less than any parameters: R_{eq}, A, B, and so on, so the deformed halfcell can be considered as an elliptic one. It is difficult to explain physically the increase of R_{eq} by stretching the cell. It is however seen that this increase of R_{eq} is less

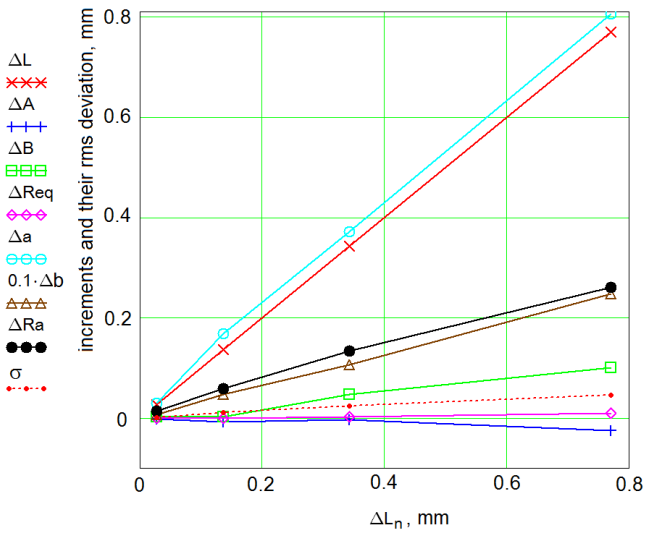

Figure 8: Residual deformation of the unstiffened halfcell vs elongation.

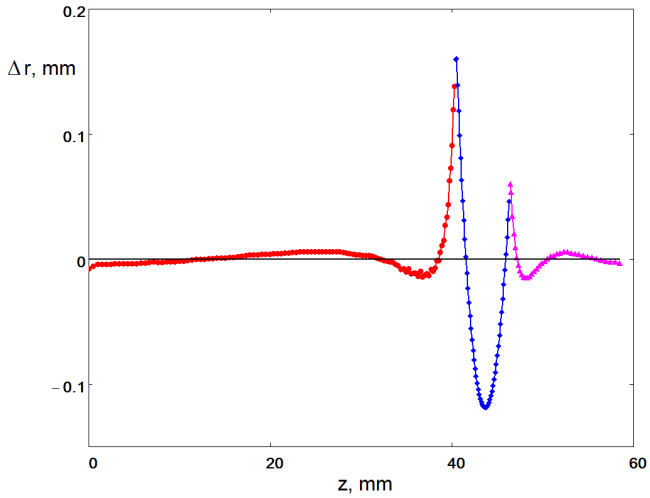

Figure 9: Deviation from the elliptic shape for the halfcell after application of 8 kN stretching force. Red line is for the equatorial elliptic arc, blue - for the straight segment, magenta - for the iris arc.

than the value of σ. This means that actually R_{eq} can not increase by stretching the cell but this apparent increase is due to rms fitting of the equatorial elliptic arc, see also Fig. 9. Let's note that the increment Δb in Fig. 8 is decreased 10 times to make the graph more compact. The bisector ΔL vs ΔL is also shown to highlight that the elongation of the halfcell happens mainly due to the increase of the half-axis a.

Deviation from the "ideal" elliptic cavity shape, consisting of 2 elliptic arcs connected with a straight segment, is shown in Fig. 9 for the stretching force of 8 kN. One can see that the maximal deformation occurs near the transion from the equatorial arc to the straight segment.

The change of the working frequency of the halfcell also

Table 1: Coefficients of proportionality for the dimensions and frequency changes with elongation and compression of the halfcell as a part of the dumbbell and as a part of the end group.

		$\Delta A/\Delta L$	$\Delta B/\Delta L$	$\Delta R_{eq}/\Delta L$	$\Delta a/\Delta L$	$\Delta b/\Delta L$	$\Delta R_a/\Delta L$	$\Delta f/\Delta L$
Unstiffened	Elongation	-0.0372	0.108	0.0109	1.057	3.202	0.349	4.15 MHz/mm
dumbbell	Compression*	2.11	3.80	-0.432	-0.434	-1.650	0.0474	6.62 MHz/mm
Stiffened	Elongation	1.662	nonlinear	-0.603	0.250	nonlinear	-0.024	6.18 MHz/mm
dumbbell	Compression*	0.564	-4.69	-1.307	-0.0190	-0.0671	0.0319	7.19 MHz/mm
Unstiffened	Elongation	0.0119	0.463	0.0126	3.205	18.8	0.189	4.49 MHz/mm
end group	Compression*							
Stiffened	Elongation	1.505	nonlinear	-0.593	0.1260	nonlinear	0.0289	7.26 MHz/mm
end group	Compression*							

*For compression ΔL is negative.

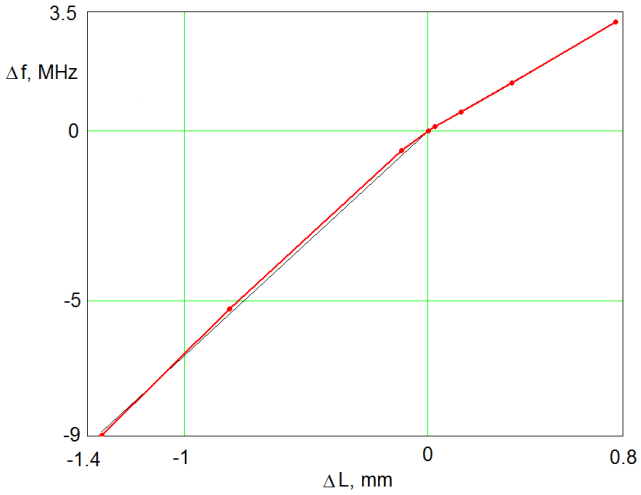

Figure 10: Shift of the working frequency of the unstiffened halfcell vs elongation and compression. Points are simulated by ANSYS, the thin black line is a linear approximation.

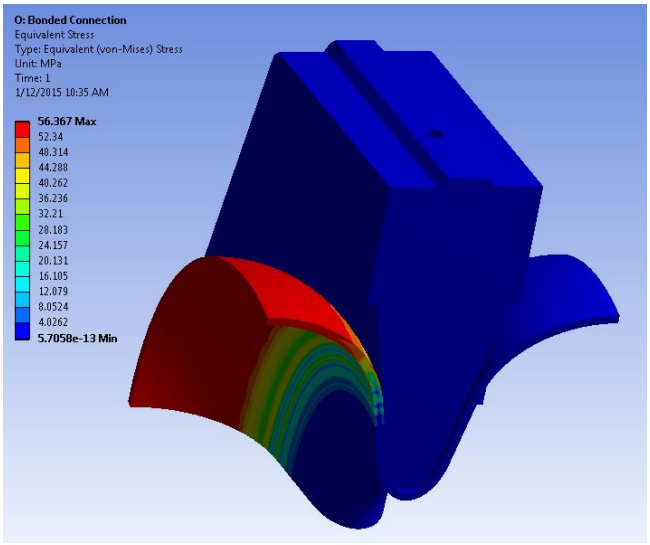

Figure 11: Dumbbell with the tuner die.

appears linear with ΔL, as is shown in Fig. 10. Points are the calculated frequencies for the found deformations, the line is the linear approximation. The coefficients of proportionality for the dimensions and frequency changes for elongation are presented in Table 1. The value of $\Delta f/\Delta L = 4.15$ MHz/mm is comparable with the values mentioned in the Introduction but relations between the increments of geometrical parameters defining the halfcell differ from both the simplified model [4] and from the data for elastic deformations presented in [2].

The frequency change is defined for the individual halfcell limited by the electric wall in the equatorial plane and by the magnetic wall in the iris plane. The measured frequency shift when the halfcell is incorporated into the multicell cavity will be of course different from this value. The actual influence on the multicell cavity frequency can be calculated with SLANS or another specialized software.

In reality, for stretching the special dies are used as will be described in the next section. So, not only the stretched cell is deformed but the adjacent cells on both external sides of the die also. More detailed calculations are needed to analyze deformation of these cells.

COMPRESSING AN INNER CELL WITHOUT STIFFENING RINGS

For compressing the cell with the goal of decreasing its frequency, the cell was squeezed between two special dies. Because of symmetry only one die and one half of the compessed cell was used in the simulation as it is shown in Fig. 11. The die moves parallel to the cavity axis to the left, the left halfcell is fixed in the equatorial plane but can expand or shrink radially in this plane. To secure the rigidity of the iris area, the model includes the whole dumbbell as in the above section.

As can be seen in Fig. 12, the force needed for the same

deformation as in the case of stretching is about 4 times larger. This is because now the equator area having larger cross-section is deformed rather than the iris area.

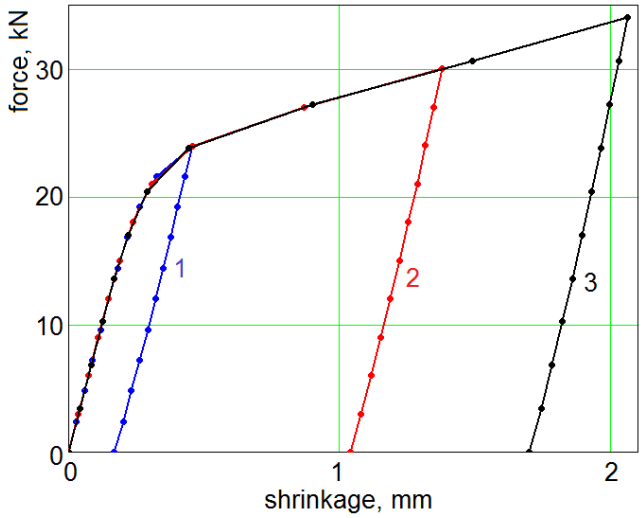

Figure 12: Elasto-plastic behavior of the halfcell as part of a dumbbell for maximal compressing force 24, 30, and 34 kN (1, 2, 3).

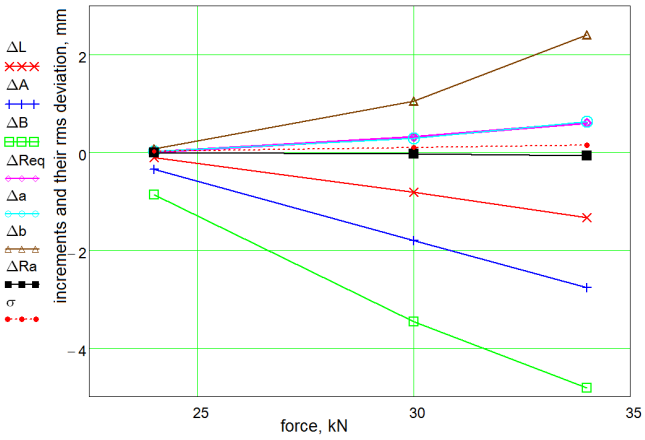

Figure 13: Residual deformation of the unstiffened halfcell vs compression.

The increments of the geometric parameters of the halfcell under compression are shown in Fig. 13. Coefficients of proportionality for linear approximations versus halfcell length increment ΔL are in the Table 1.

Deviations from the elliptic halfcell shape after application of 34 kN compressing force is shown in Fig. 14. Now deformation of the equatorial arc is comparable with the deformation of the transition between the straight segment and the arcs, cf. Fig. 9.

Frequency change under compression is shown together with the change under stretching, in Fig. 9. Let us note that though for stretching the frequency change is practically linear, there is a smooth transition to a steeper slope of the curve for compression. The linear approximation

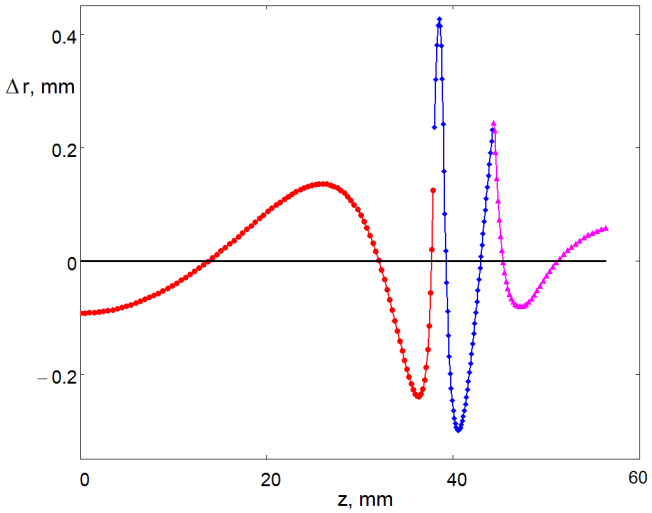

Figure 14: Deviation from the elliptic shape for the halfcell after application of 34 kN compressing force.

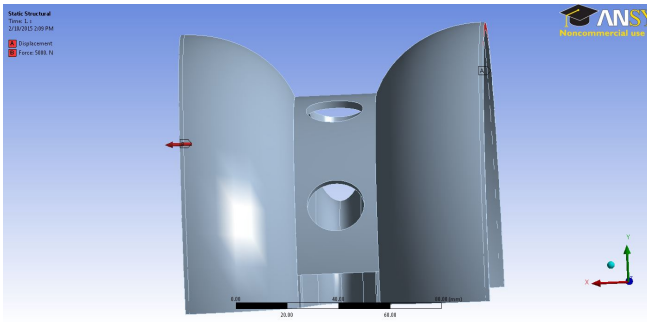

Figure 15: The model for simulation of the stiffened dumbbell.

with $\Delta f/\Delta L = 6.62$ MHz/mm (see the Table 1) is not very accurate near $\Delta L = 0$.

From the data presented in Table 1 we can conclude that frequency increase under stretching is due mainly to the increase of the distance between the consecutive irises and increase of R_a. Both changes decrease the capacitive part of the resonator. The value of R_{eq} keeps practically constant. Under compression, both the gap decrease and the R_{eq} increase (increase of the capacitive and inductive components) are responsible for the decrease of the frequency. This observations give more detail to the results presented in [7] where the frequency decrease was related to the increase of the equatorial radius.

As it was mentioned in the previous section, the adjacent cells can be also deformed when a cell is sqeezed between two dies, mainly in the iris area. This is also a subject of further research.

STRETCHING AN INNER CELL WITH STIFFENING RINGS

The model for simulation of the dumbbell with a stiffening ring is shown in Fig. 15.

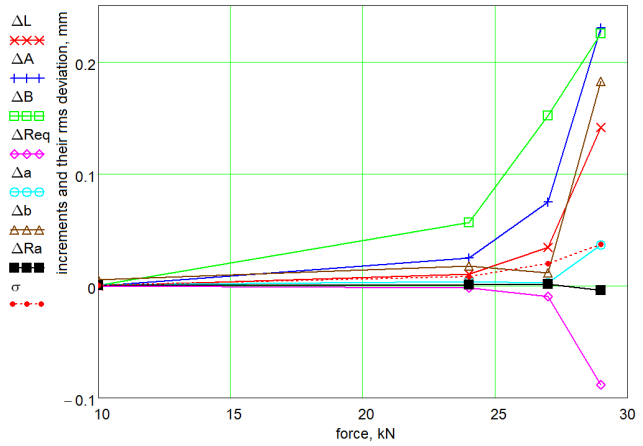

Figure 16: Residual deformation of the stiffened halfcell vs applied stretching force.

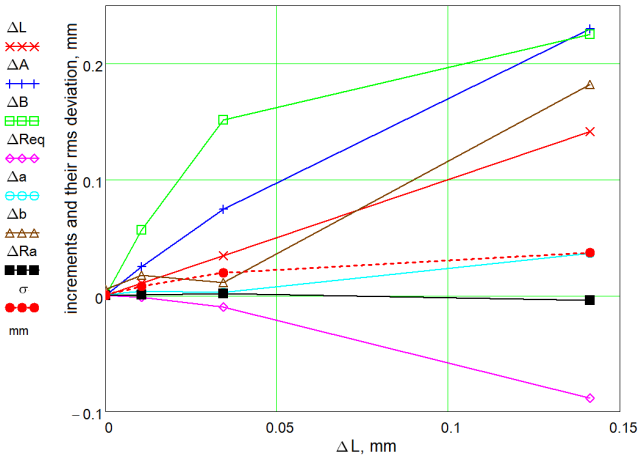

Figure 17: Residual deformation of the stiffened halfcell vs elongation.

Simulation results of stretching of the stiffened halfcell are presented in Figs. 16, 17 and in Table 1. One can see that dependences of ΔB and Δb on ΔL are not linear anymore but are close to linear for other increments.

COMPRESSING AN INNER CELL WITH STIFFENING RINGS

Residual deformation of the stiffened dumbbell after compressing by 40 kN is shown in Fig. 18. Coefficients for linearization of increments versus change of the halfcell length are presented in the Table 1. Graphs for increments of the geometric parameters versus applied compressing force are shown in Fig. 19. A distinctive feature of this graph is a lengthening (not shortening under compressing force) of the halfcell when the force is below 30 kN. The cause of this behavior is not fully understood, possibly this is because the contact between the die and the cell is point-like at the first moment when the force is small, possibly the mesh is too large (1 mm). Anyway, this anomalous behavior happens at the level less than 10 micrometers, and if the level of tuning is of the order of 100 kHz, the dependencies of the geometrical increments and Δf on ΔL are quite linear, see Figures 20 and 21.

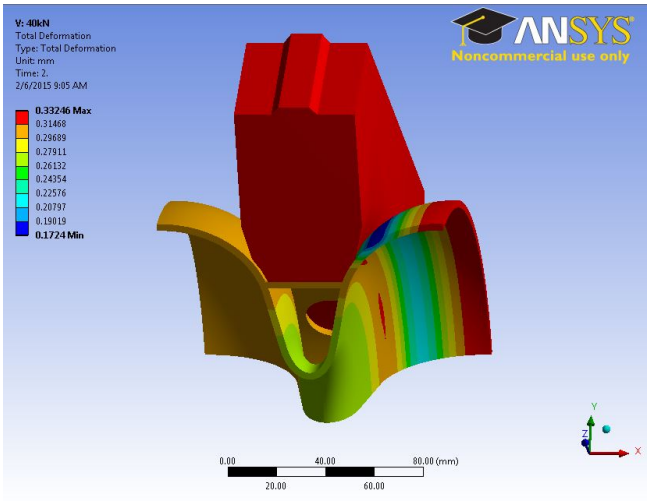

Figure 18: Residual deformation of the stiffened inner halfcell after compressing by 40 kN.

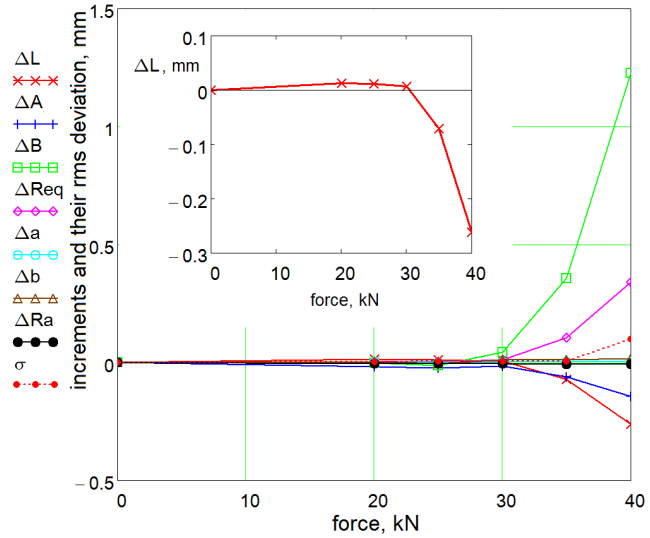

Figure 19: Residual deformation of the stiffened inner halfcell vs applied compressing force.

STRETCHING OF THE UNSTIFFENED END GROUP

Results of stretching simulations of the unstiffened end group are shown in Figs. 22 - 26 and in the Table 1. In Fig. 26 Δa and Δb seem nonlinear with ΔL. This can be an effect of the short arc when the curvature is the same for two different arcs, radius of curvature $r_c = a^2/b = const$. A small deviation of the external points of the dumbbell surface can cause a big deviation in a and b but simultaneously. The curvature keeps for a given elongation if these

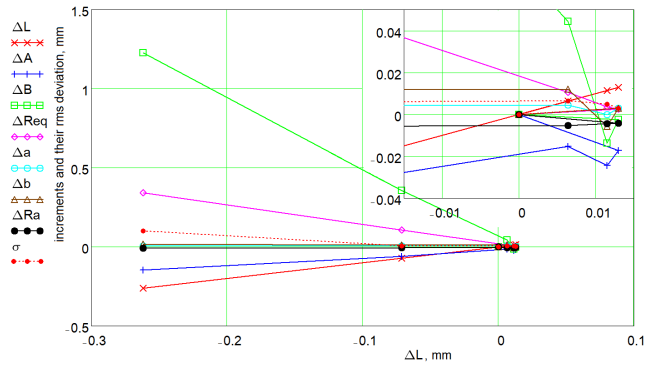

Figure 20: Residual deformation of the stiffened inner halfcell vs change of halfcell length.

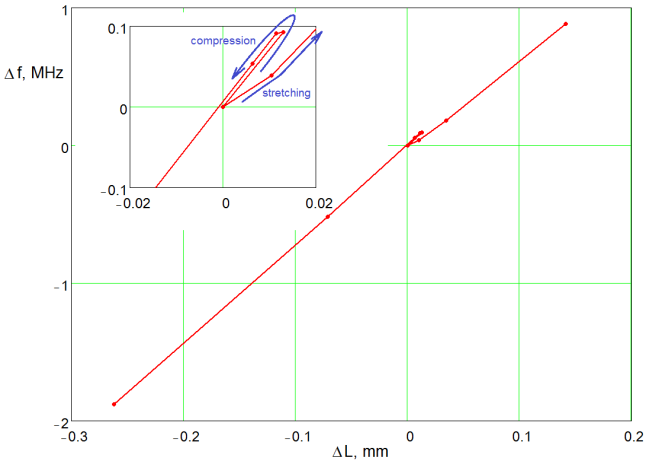

Figure 21: Shift of the working frequency of the stiffened inner halfcell vs elongation and compression.

errors in a and b are small. It varies linearly with the halfcell elongation, see the lower line in Fig 26.

Dependence of the halfcell frequency on the elongation is shown in Fig. 27. The linear dependence of frequency on the elongation is not kept for high values of ΔL. However,

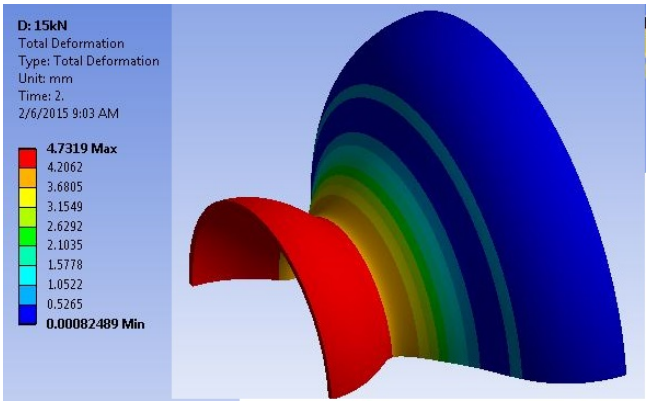

Figure 22: Residual deformation of the unstiffened end group after stretching by 15 kN.

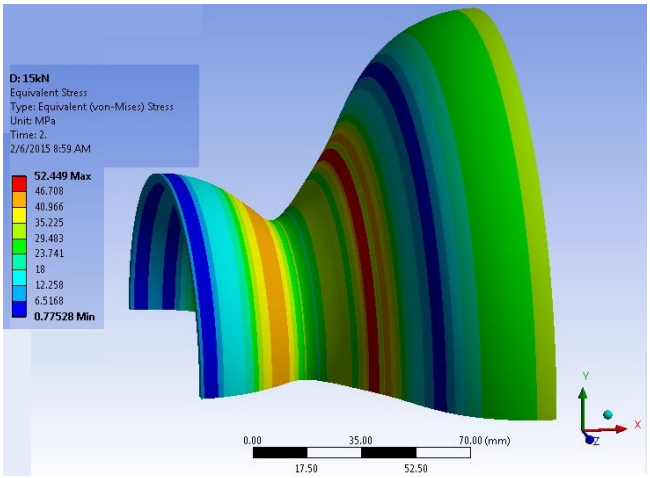

Figure 23: Residual stress of the unstiffened end group after stretching by 15 kN.

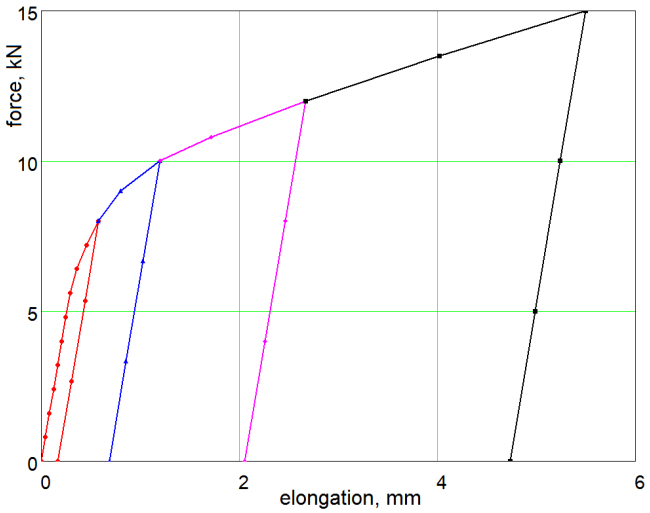

Figure 24: Elasto-plastic behavior of the unstiffened end group for maximal stretching force from 8 to 15 kN.

we do not expect the deformations as big as more than 2 mm with frequency change about 10 MHz. So, the coefficient $\Delta f/\Delta L = 4.49$ MHz/mm in the Table 1 is calculated for this initial part of the plot. Here, as it was done above for the dumbbell, we define the frequency of the halfcell when it is limited with the electric boundary in the equatorial plane and with the magnetic boundary in the iris plane.

COMPRESSING OF THE UNSTIFFENED END GROUP

This work was not finished because of lack of financing.

STRETCHING OF THE STIFFENED END GROUP

Residual deformation of the stiffened end group after stretching by 30 kN are shown in Fig. 28. Elasto-plastic

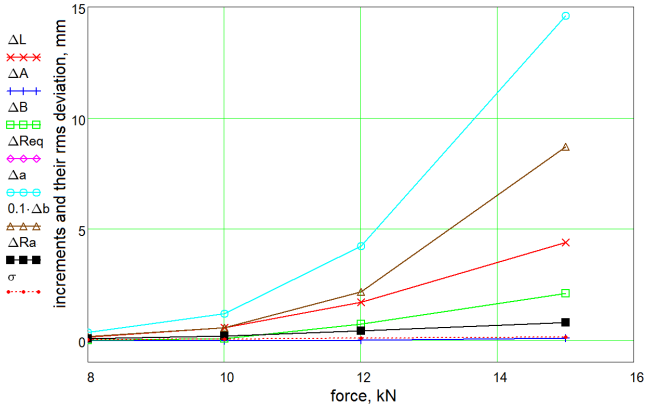

Figure 25: Residual deformation of the unstiffened end group halfcell vs applied stretching force.

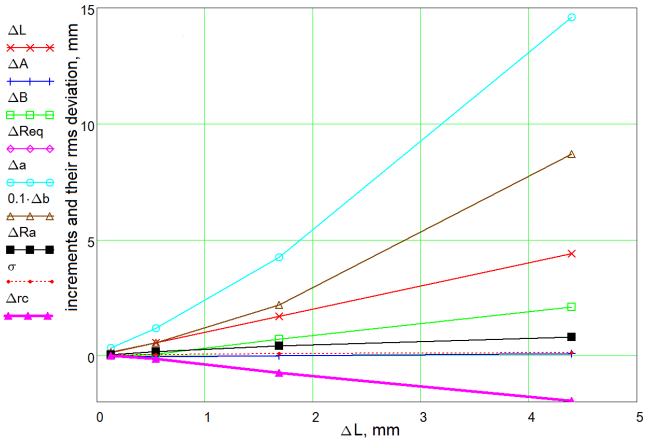

Figure 26: Residual deformation of the unstiffened end group halfcell vs elongation.

behavior of the stiffened end group for maximal stretching force from 10 to 30 kN is presented in Fig. 29. One can see that no residual deformation occurs at 10 kN and up to approximately 14 kN.

COMPRESSING OF THE STIFFENED END GROUP

This work was not finished because of lack of financing.

CONCLUSION

Tuning of a multicell superconducting cavity with the goal to compensate errors of manufacturing and to obtain necessary field flatness between the cells is used in any laboratory working with these cavities as a part of the cavity preparation. The present work, to the best of our knowledge, is the first attempt to connect forces for this tuning with changes of dimensions and frequency, to find limits of elastic and plastic deformations. Simulations were done with the ANSYS software. Properties of niobium used for the simulations were chosen from a variety of data, actually they are different depending on the preparation of the

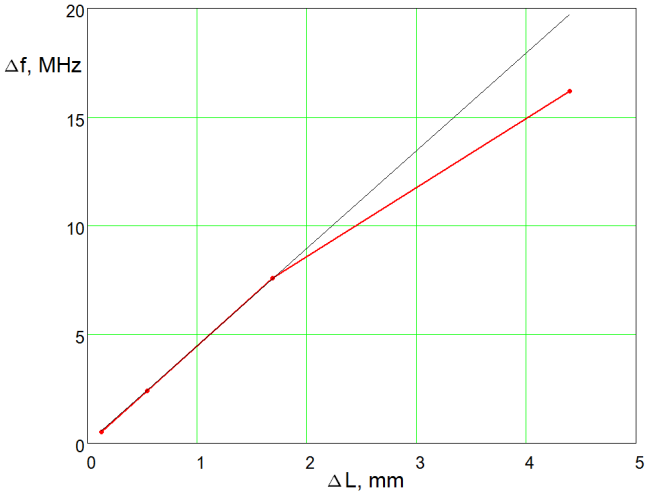

Figure 27: Frequency shift of the halfcell in the unstiffened end group vs elongation. Calculated points and a linear approximation.

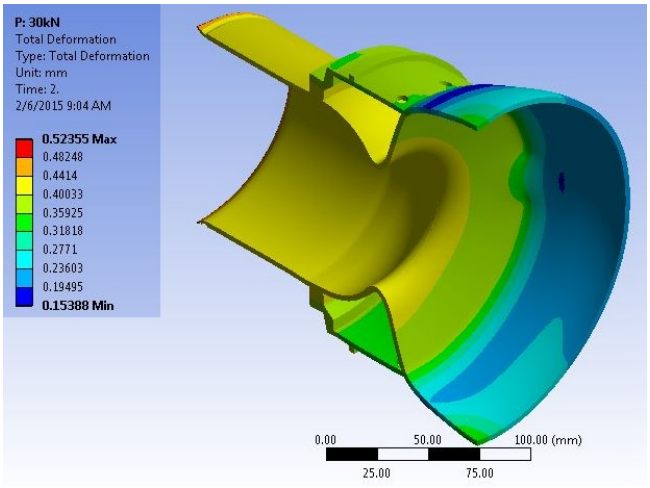

Figure 28: Residual deformation of the stiffened end group after stretching by 30 kN.

material, but we hope that the main dependences will be qualitatively the same for any quality of the metal. Usage of stiffening rings needed for limitation of the Lorentz forces when a cavity works with strong fields, changes significantly its mechanical properties. These simulations are done for the inner cells but were not finished for the end group.

It is shown that the shape of the cavity cell, inspite of its deformations, can be treated with a good accuracy as an elliptic shape. In this case, it is easy to calculate frequency change versus the cell elongation or shortening, using a special software, e. g. SLANS [8]. The correct account of the shape change gives a way for calculation of higher order modes. It is shown that a simplified approach to the deformations used earlier leads to unreliable results. It is found that the change of the geometrical parameters of the cavity cell, half-axes of the elliptic arcs, equatorial

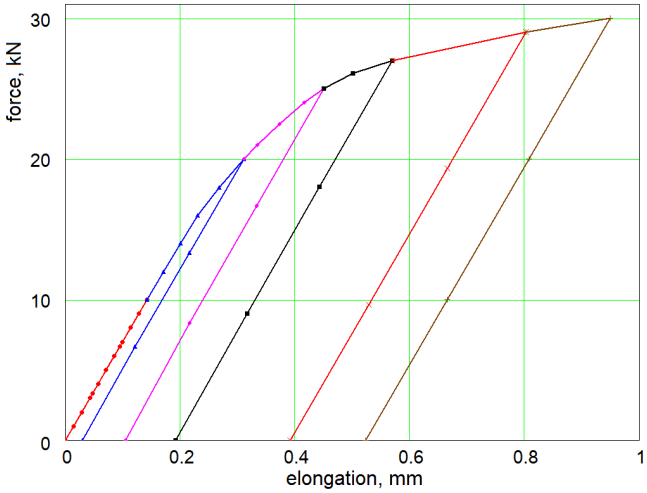

Figure 29: Elasto-plastic behavior of the stiffened end group for maximal stretching force from 10 to 30 kN.

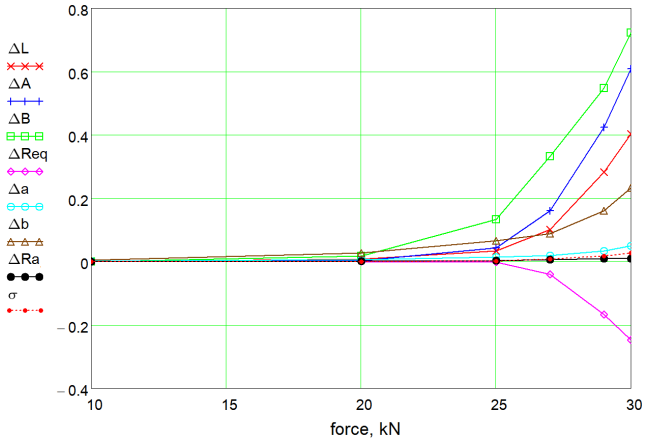

Figure 30: Residual deformation of the stiffened end group halfcell vs applied stretching force.

and aperture radii, its working frequency, are in most cases linear function of the increment of the cavity length.

ACKNOWLEDGMENT

The authors are thankful to Tim O'Connel, James Sears, John Kauffman, Joshua Robbins and to other colleagues for their help and useful discussions.

REFERENCES

[1] Hasan Padamsee et al. *RF superconductivity for accelerators*. John Wiley & Sons, 1998.

[2] Valery Shemelin and Paul Carrier. Frequency control in the process of a multicell cavity production. Rev. Sci. Instrum. **81**, 043304 (2012); `http://dx.doi.org/10.1063/1.4705985`.

[3] James Sears. Private communication.

[4] Nicholas Valles. Dissertation. Cornell University, 2014.

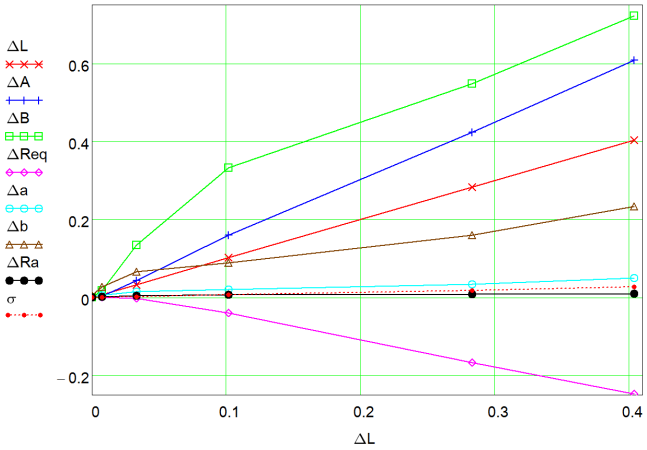

Figure 31: Residual deformation of the stiffened end group halfcell vs elongation.

[5] `http://www.ansys.com/`

[6] G. Wu, H. Edwards, T. Peterson. Summary of Niobium mechanical properties. Fermilab, 2008. `http://ilc-dms.fnal.gov/Workgroups/CryomoduleDocumentation/3rd-Harmonic-Cryomodule-for-DESY...`

[7] F. Marhauser. JLab SRF cavity fabrication errors, consequences and lessons learned. (TJNAF, Newport News, VA, 2010), Paper No. JLab-TN-10-021.

[8] `http://www.euclidtechlabs.com/SLANS/slans.php`